ESRF	**Experiment title:** Ultra-fast diffraction imaging of brittle fracture crack initiation	**Experiment number**: MA-5714
Beamline: ID19	**Date of experiment**: from: 31 July 2023 to: 02 August 2023	**Date of report**: 13/09/2023
Shifts: 6	**Local contact(s)**: Alexander Rack, Bratislav Lukic	*Received at ESRF:*

Names and affiliations of applicants (* indicates experimentalists):

***François Rieutord, SOITEC**

***Samuel Tardif, CEA**

***Pablo Acosta Alba, CEA**

***Lucas Colonel, CEA**

***Frederic Mazen, CEA**

***Katell Blanco, CEA (PhD student)**

Report:

The experiment MA5714 was conducted as initially planned. Our previous results were recently published[1] and highlight in a "technical spotlight" by the ESRF[2]. Now that we have shown that we could image the fracture propagating at several km/s in a brittle material, we set up here a similar experiment, trying now to look at the early stages of the fracture, just after its initiation. We used the fast scintillator, image intensifier and ultra-fast camera (Shimadzu) available at ID19. We improved our IR led setup for the crack, using now lenses mounted on a fixed plate (Fig. 1). As a result, the IR alignment for each sample was much faster, increasing the overall throughput of the experiment.

We confirmed that the heatload on the sample in 4-bunch mode, using two undulators and a wiggler, was enough to heat the sample much over 350°C and initiate the fracture. The exact temperature values have not been recovered yet, as our laptop connected to the thermocouple array inside the experimental hutch broke down unexpectedly during the experiment. We note for future experiments to either better shield the laptop with lead, or use a remote connection the thermocouple reader using the cable passthrough. In the strip geometry that we used, the sample size was about 100-300 mm x 30 mm, much larger than the irradiated area. In order to reduce the heat loss (mostly by air convection), we had to wrap the samples in aluminum foil, leaving openings for the X-ray and IR beams (Fig. 2).

We performed the measurements as planned, on Si wafers that were assembled with a twist angle of about 45°. The reason for this was to avoid the overlapping of the diffracted images on the camera. Since the illumination of the field of view is already highly non-uniform (post-EBS), processing two overlapping images was deemed too complicated.

[1] A. Petit *et al., J. Appl. Cryst.* **55**, 911-918 (2022), https://scripts.iucr.org/cgi-bin/paper?S1600576722006537

[2] https://www.esrf.fr/home/news/tech-talk/content-news/tech-talk/techtalk12.html

The 4-bunch mode used resulted in a pulsed illumination (stroboscopic), with a period of 704 ns between pulses. For our purposes, the bunch length can be considered instantaneous. At the time of each bunch, the diffracted image is imprinted on the scintillator screen of the image intensifier. The scintillator intensity is proportional to the X-ray intensity and decays over time, at first quite rapidly and then much more slowly. As a result, the "clock" of the experiment is set by the timing of the bunch, while the image recording is driven by the camera. If the exposure time of the camera is close to a multiple of the pulse period, then the full decay between two consecutive pulses is measured and the intensity is constant. On the contrary, if the exposure is very different from a multiple of the pulse period, a "beating" phenomena can appear and the intensity can vary wildly from image to image, even without any changes in the sample, preventing a quantitative image-to-image analysis, unless proper normalization is performed.

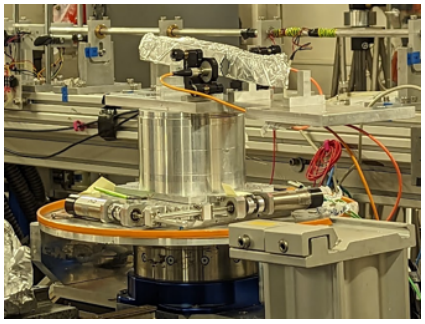

Fig. 1: Sample mounted on the holder with the IR fracture detection system plate.

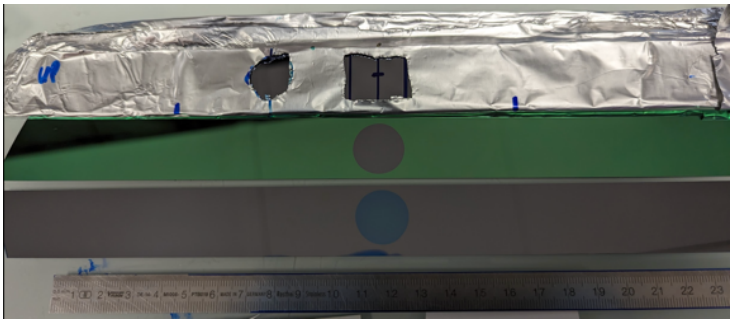

Fig. 2: (top) Typical strip sample, wrapped in Al foil to minimize heat loss by air convection. (middle) Fractured sample. (bottom) Ruler, for scale.

The pulses can be phased with the camera recordings by plotting the intensity in the image, as a function of the time of recording modulo the (known) pulse period, while the sample is still not fractured and the diffraction is expected to be constant (Fig. 3). Then the time offset between the first pulse and the first image recorded can be computed, and a common timescale for pulse arrival and image recording can be established. Figure 4 shows the pulse train and the camera exposure gate train on a common timescale, for a selected timeframe. In this particular example, image #116 is recording the scintillator response to the pulse #81, while image #117 is recording that of pulse #82. Even if the two images are only 500 ns apart, the physical signal they record are 704 ns apart (one pulse period). Image #118 is an overlap of pulse #82 and #83, and so on.

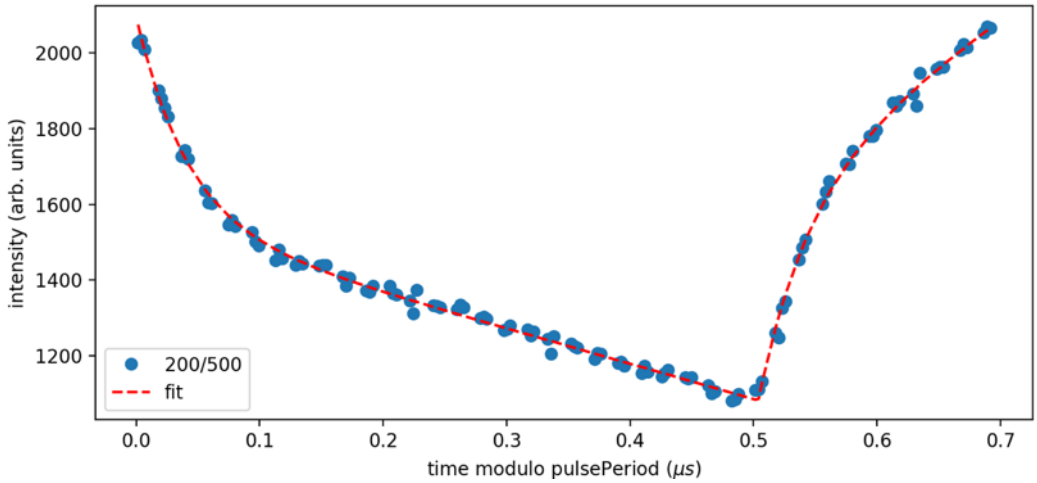

Fig. 3: Image intensity as a function of time modulo the pulse period (704 ns) for the images before the crack and corresponding fit using a double decay model for the scintillator impulse response function.

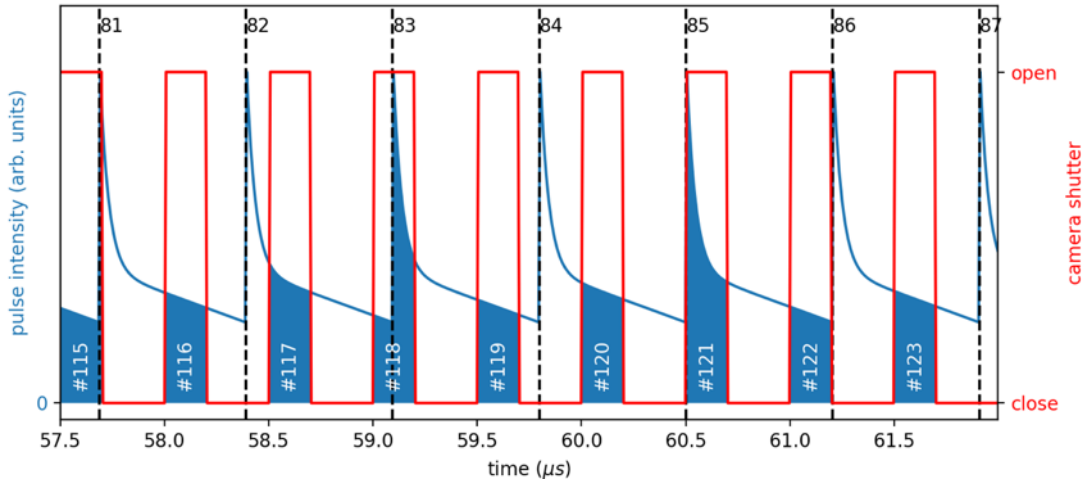

Fig. 4: (black dashed lines and numbers) Individual pulses from the 4-bunch mode on a time scale, restricted here to a timeframe of interest. (blue lines) Scintillator response to the pulse exposure, showing a fast and then slow decay. (red line) Gate exposure of the camera, in this example the camera is exposed 200 ns every 500 ns. The filled blue area under each gate function indicates the integrated signal from the scintillator and the white number indicates the image number.

The scintillator decay can then be corrected for, and the recorded intensity normalized, thus allowing an image-to-image quantitative analysis (Fig. 5).

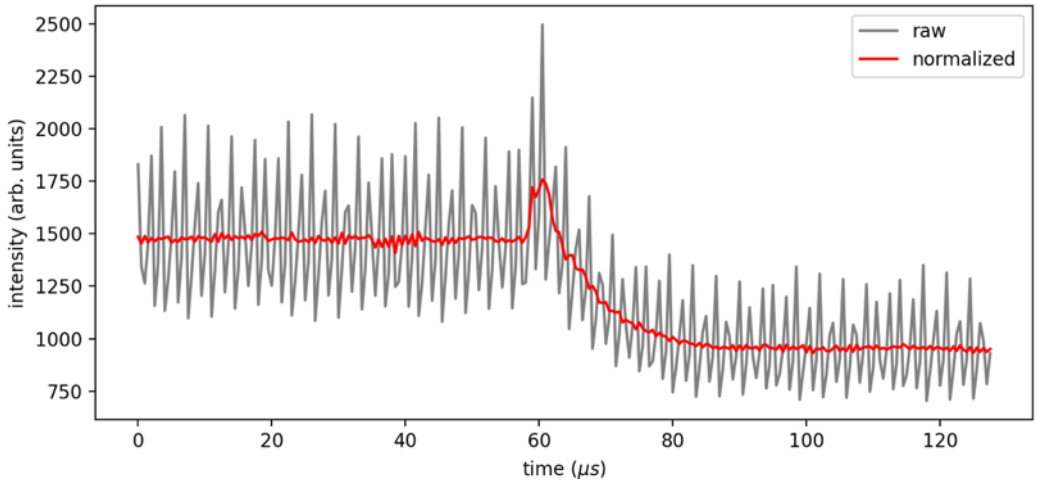

Fig. 5: Raw image intensity as a function of time (grey line), and corrected intensity considering the scintillator impulse response function and the time offset between the pulses and the image recording.

A typical result is shown in Fig. 6. The effect of the fracture is quite clear in the total intensity (at about 60 µs in Fig. 5), yet it is not obvious in the raw data (Fig. 5, grey line, and Fig. 6, left column) due to the intensity oscillations for these recording parameters. Once the intensity is corrected, the fracture and the crack front propagation can be evidenced in the differential imaging, considering either the last image before the fracture (#115) as a reference, or the previous image. No propagation seems to occur in image #119, which is expected since it images the same pulse as the previous one. More surprisingly, image #120 also shows no change. At the moment we suspect that the crack front is located in the "blind" area of the illumination field, as seen by the two very-low intensity lobes around the center peak.

The in-depth analysis of our data to study the dynamics of the crack front propagation is under way. We have successfully recorded the initiation and propagation of the crack in several samples, in a very reproducible way. Thus, we could test various acquisition parameters (namely exposure time and frame rate) and the ongoing analysis will help determining the optimal parameter set. The ability to trigger the fracture only with heatload

from the 4-bunch mode was confirmed, which means that any filling mode could be used for this kind of imaging. In particular, we foresee that 16-bunch imaging in the same conditions could provide better time-resolved data, in line with the technical specification of the ultra-high-speed camera available at ID19.

Continuous help and support from the ID19 beamline staff are gratefully acknowledged.

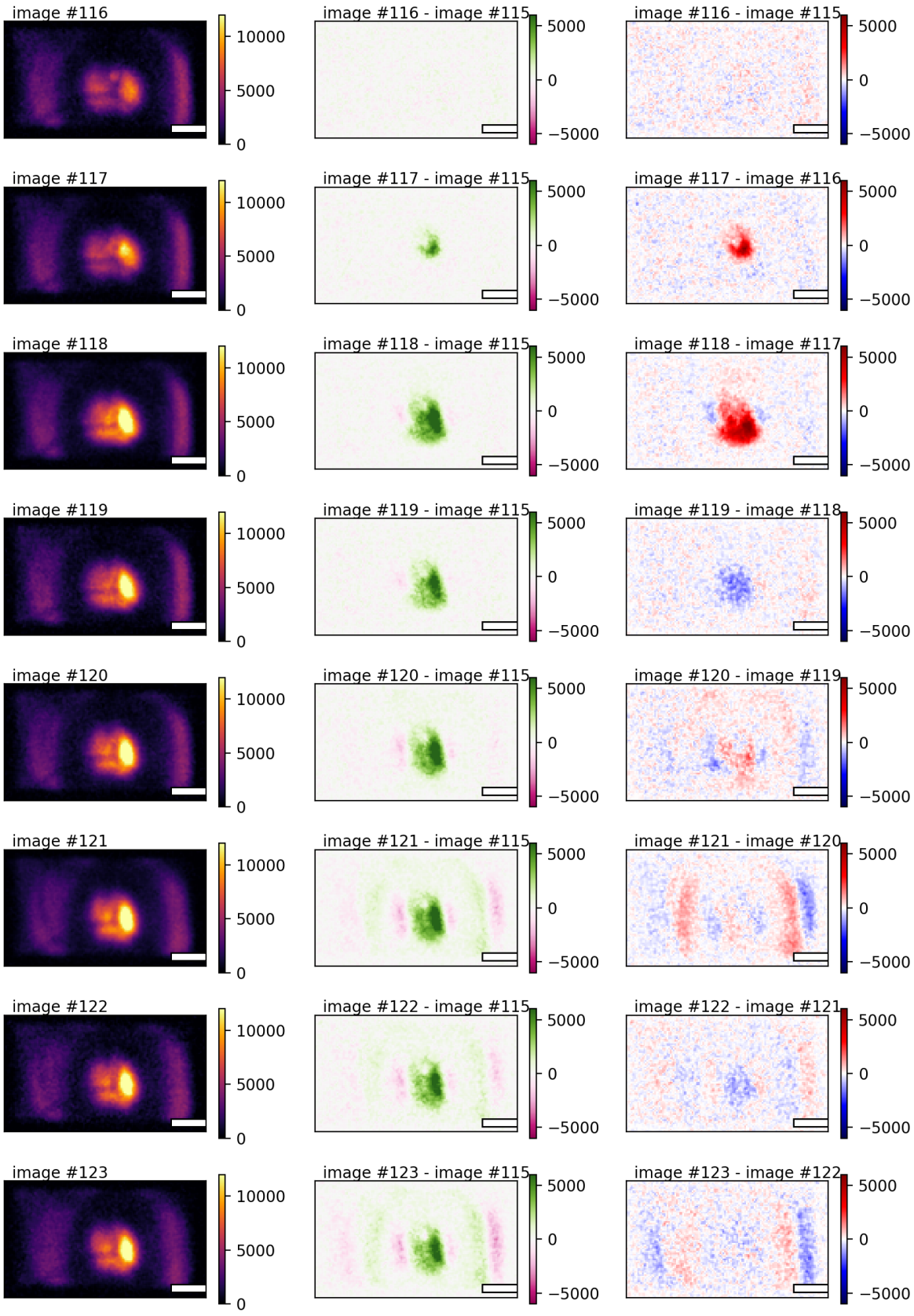

Fig. 6: (left column) Raw diffraction image. (middle column) Difference to the last image before the fracture was detected. (right column) Image-to-image difference (derivative imaging).